

An SQP Method Combined with Gradient Sampling for Small-Signal Stability Constrained OPF

Peijie Li, *Member, IEEE*, Junjian Qi, *Member, IEEE*, Jianhui Wang, *Senior Member, IEEE*, Hua Wei, Xiaoqing Bai, and Feng Qiu

Abstract—Small-Signal Stability Constrained Optimal Power Flow (SSSC-OPF) can provide additional stability measures and control strategies to guarantee the system to be small-signal stable. However, due to the nonsmooth property of the spectral abscissa function, existing algorithms solving SSSC-OPF cannot guarantee convergence. To tackle this computational challenge of SSSC-OPF, we propose a Sequential Quadratic Programming (SQP) method combined with Gradient Sampling (GS) for SSSC-OPF. At each iteration of the proposed SQP, the gradient of the spectral abscissa function is randomly sampled at the current iterate and additional nearby points to make the search direction computation effective in nonsmooth regions. The method can guarantee SSSC-OPF is globally and efficiently convergent to stationary points with probability one. The effectiveness of the proposed method is tested and validated on WSCC 3-machine 9-bus system, New England 10-machine 39-bus system, and IEEE 54-machine 118-bus system.

Index Terms—small-signal stability, AC optimal power flow (ACOPF), gradient sampling, nonsmooth optimization, sequential quadratic programming, spectral abscissa.

I. INTRODUCTION

IN the large interconnected power systems, the small-signal stability problem with the oscillation behavior can greatly threaten the system security [1]. The increased penetration of renewable energy sources can further deteriorate the small-signal stability [2]–[4], which is mainly driven by:

- 1) Converter control-based generators including variable-speed doubly fed asynchronous generators and photovoltaic (PV) plants are replacing the conventional generators. These solid-state inverters, however, usually do not contribute to the system inertia [2].
- 2) The fluctuating nature of the renewable resources such as wind and solar may cause rapid changes in future generation patterns, leading to rapid fluctuations of the power system's operating point [3].
- 3) In some countries, such as China, due to the differences between the geographical distribution of load center and renewable energy, new Ultra-high-voltage Alternating

This work was supported in part by National Natural Science Foundation of China under Grant 51407036, 51367004, the National Basic Research Program of China (973 Program) under Grant 2013CB228205 and the U.S. Department of Energy (DOE)'s Office of Electricity Delivery and Energy Reliability.

P. Li is with the College of Electrical Engineering, Guangxi University, Nanning, 530004 China. He is visiting Argonne National Laboratory, Lemont, IL 60439 USA (e-mail: lipeijie@gxu.edu.cn).

J. Qi, J. Wang, and F. Qiu are with Energy Systems Division, Argonne National Laboratory, Lemont, IL 60439 USA (e-mails: jqj@anl.gov; jianhui.wang@anl.gov; fqiu@anl.gov).

H. Wei and X. Bai are with the College of Electrical Engineering, Guangxi University, Nanning, 530004 China.

Current (UHVAC) transmission lines are built to transfer the clean energy. The long distance power transmission over these UHVAC lines can result in oscillations [4].

Although the damping controllers can enhance small-signal stability, they cannot always guarantee the system to be small-signal stable [5]. By contrast, re-dispatch can provide additional stability measures and control strategies to make the system to be small-signal stable. Most commercial software, such as PSS[®]E and NEPLAN, only uses participation factors [6], [7] to perform offline re-dispatch study. Nonetheless, participation factors can neither determine whether the generation for each generator should be increased or decreased, nor tell how much generation should be dispatched [8]. On the contrary, the Small-Signal Stability Constrained Optimal Power Flow (SSSC-OPF) is a commendable model that can give the complete re-dispatch information to guarantee the small-signal stability while considering the economic objective and technical constraints. However, solving the SSSC-OPF problem can be very challenging because of the nonsmooth nature of the small-signal stability constraint. Existing methods for solving SSSC-OPF include:

- Numerical eigenvalue sensitivity based Interior Point Method (IPM): Numerical eigenvalue sensitivities have been used to improve the power transfer capability constrained by small-signal stability [5]. In [9], an SSSC-OPF is formulated to achieve an appropriate security level under stressed loading conditions, in which the small-signal stability constraint is replaced by first-order Taylor series expansion and the gradients of the real part of the critical eigenvalue are computed by numerical eigenvalue sensitivities. This method tries to make the small-signal stability constraint feasible by successively solving SSSC-OPF with IPM, but it may compromise on the economic cost due to losing the high-order terms of the small-signal constraint.
- Approximate singular value sensitivity based IPM: An SSSC-OPF is used to tune the oscillation controls in electricity markets [10], in which the minimum singular value of the modified full Jacobian matrix is proposed as a stability index. However, the gradient of this index is derived approximately by first-order Taylor series expansion and the Hessian is numerically evaluated by perturbing the gradients.
- Closed-form eigenvalue sensitivity based IPM: An expected-security-cost OPF with the small-signal stability constraint is presented in [11], in which a more computational efficient closed-form formula is used to calculate the eigenvalue sensitivities [12], [13]. Nevertheless, the

second-order eigenvalue sensitivities essential for forming the Hessian of the small-signal stability constraints for IPM have to be derived and calculated, which can be very time-consuming.

- Nonlinear semi-definite programming (NLSDP) method: A nonlinear semi-definite programming model is proposed to formulate the spectral abscissa constraint as a semi-definite constraint indirectly which is further transformed to some smooth nonlinear constraints [14]. An explicit and equivalent small-signal stability constraint is obtained based on Lyapunov theorem. However, the dense subsidiary semi-definite matrix variables may make the model computationally prohibitive for large systems.

IPM methods cannot guarantee convergence of SSC-OPF, even locally, because of the nonsmooth nature of the small-signal stability constraint function. During iterations they may suffer from oscillations between critical modes for different generator rescheduling patterns. Recently, a Sequential Quadratic Programming (SQP) method combined with Gradient Sampling (GS), called SQP-GS, is proposed for the nonsmooth constrained optimization [15]. Based on the SQP-GS, this paper proposes an optimization method to solve the SSSC-OPF problem with global convergence. The closed-form eigenvalue sensitivity is used to calculate the gradient of the spectral abscissa. Since the SQP only needs the gradients of all functions in the model, the second-order eigenvalue sensitivities are not needed. Moreover, owing to only one nonsmooth function in SSSC-OPF, GS can be performed only for this nonsmooth function, which would be beneficial to improve computation efficiency significantly.

The remainder of this paper is organized as follows. Section II describes the small-signal stability model. In Section III, the property of the small-signal stability constraint and the calculation of the eigenvalue sensitivities are discussed. Section IV introduces the SQP-GS method for nonsmooth constrained optimization. Then we discuss how to solve the SSSC-OPF problem by the SQP-GS method in Section V. The proposed method is tested and validated on three systems in Section VI. Finally the conclusion is drawn in Section VII.

II. SMALL-SIGNAL STABILITY MODEL

A. General Model of Small-Signal Stability

The behavior of a dynamical system can be described by differential and algebraic equations in the following form

$$\dot{\mathbf{s}} = \mathbf{f}_d(\mathbf{s}, \mathbf{u}, \mathbf{y}) \quad (1)$$

$$\mathbf{0} = \mathbf{f}_a(\mathbf{s}, \mathbf{y}), \quad (2)$$

where \mathbf{s} is the vector of state variables, \mathbf{u} is the vector of inputs, and \mathbf{y} is the non-state variables.

In small-signal stability analysis, the linearized form of (1)–(2) is often used:

$$\begin{bmatrix} \Delta \dot{\mathbf{s}} \\ \mathbf{0} \end{bmatrix} = \begin{bmatrix} \tilde{\mathbf{A}} & \tilde{\mathbf{B}} \\ \tilde{\mathbf{C}} & \tilde{\mathbf{D}} \end{bmatrix} \begin{bmatrix} \Delta \mathbf{s} \\ \Delta \mathbf{y} \end{bmatrix} + \begin{bmatrix} \mathbf{E}_1 \\ \mathbf{0} \end{bmatrix} \Delta \mathbf{u}. \quad (3)$$

Eliminating $\Delta \mathbf{y}$ we can get

$$\Delta \dot{\mathbf{s}} = \mathbf{A} \Delta \mathbf{s} + \mathbf{E}_1 \Delta \mathbf{u}, \quad (4)$$

where $\mathbf{A} = \tilde{\mathbf{A}} - \tilde{\mathbf{B}} \tilde{\mathbf{D}}^{-1} \tilde{\mathbf{C}}$ is commonly referred to as the state matrix.

B. Differential and Algebraic Equations of Power Systems

1) *Generator Model*: The two-axis synchronous generator model [6] that has been widely used in small-signal stability analysis is considered in this paper. This model is more realistic than the classical model used in [16], which is appropriate only for the most basic studies. The differential equations for generator $i \in S_G$ can be written as

$$\frac{d\delta_i}{dt} = \omega_i - \omega_s \quad (5)$$

$$\frac{d\omega_i}{dt} = \frac{1}{M_i} \left(T_{Mi} - (E'_{qi} - X'_{di} I_{di}) I_{qi} - (E'_{di} + X'_{qi} I_{qi}) I_{di} - D_i (\omega_i - \omega_s) \right) \quad (6)$$

$$\frac{dE'_{qi}}{dt} = \frac{1}{T'_{dqi}} \left(-E'_{qi} - (X_{di} - X'_{di}) I_{di} + E_{fdi} \right) \quad (7)$$

$$\frac{dE'_{di}}{dt} = \frac{1}{T'_{dqoi}} \left(-E'_{di} + (X_{qi} - X'_{qi}) I_{qi} \right), \quad (8)$$

where S_G is the set of generators, δ_i is rotor angle, ω_i is rotor speed, ω_s is rated rotor speed, E'_{di} and E'_{qi} are, respectively, the d-axis and q-axis components of the internal voltage, I_{di} and I_{qi} are d-axis and q-axis components of the internal current, T_{Mi} is mechanical power output, M_i is inertia constant, D_i is damping torque coefficient, E_{fdi} is excitation output voltage, X_{di} and X_{qi} are synchronous reactance, X'_{di} and X'_{qi} are transient reactance, and T'_{dqi} and T'_{dqoi} are open-circuit time constant, respectively, at d and q axes.

Besides, the stator algebraic equations for generator $i \in S_G$ can be written in polar form as [6]

$$E'_{di} - V_i \sin(\delta_i - \theta_i) - R_{si} I_{di} + X'_{qi} I_{qi} = 0 \quad (9)$$

$$E'_{qi} - V_i \cos(\delta_i - \theta_i) - R_{si} I_{qi} - X'_{di} I_{di} = 0, \quad (10)$$

where V_i is bus voltage magnitude, θ_i is bus voltage phase angle, and R_{si} is the armature resistance.

2) *Exciter Model*: In this paper we use the IEEE Type DC-1 exciter for each generator, which can be expressed in differential equations for generator $i \in S_G$ as [6]

$$\frac{dE_{fdi}}{dt} = \frac{1}{T_{Ei}} \left(- (K_{Ei} + S_E(E_{fdi})) E_{fdi} + V_{Ri} \right) \quad (11)$$

$$\frac{dV_{Ri}}{dt} = \frac{1}{T_{Ai}} \left(-V_{Ri} + K_{Ai} R_{Fi} - \frac{K_{Ai} K_{Fi}}{T_{Fi}} E_{fdi} + K_{Ai} (V_{refi} - V_i) \right) \quad (12)$$

$$\frac{dR_{Fi}}{dt} = \frac{1}{T_{Fi}} \left(-R_{Fi} + \frac{K_{Fi}}{T_{Fi}} E_{fdi} \right), \quad (13)$$

where V_{Ri} is voltage regulator output, R_{Fi} is exciter rate feedback, $S_E(E_{fdi}) = A_{ei} e^{B_{ei} E_{fdi}}$ is the field saturation function with coefficients A_{ei} and B_{ei} , K_{Ei} is exciter gain, K_{Ai} is voltage regulator gain, K_{Fi} is rate feedback gain, T_{Ei} is exciter time constant, T_{Ai} is voltage regulator time constant, T_{Fi} is rate feedback time constant, and V_{refi} is the reference voltage.

3) *Network Model*: The network equations relate the real and reactive power injections at each bus to the voltage magnitudes and phase angles at the system buses. In this paper the loads are modeled as constant power. Then for a generator bus $i \in S_G$ we have [6]

$$I_{di}V_i \sin(\delta_i - \theta_i) + I_{qi}V_i \cos(\delta_i - \theta_i) + P_{Li} - \sum_{j \in S_B} V_i V_j Y_{ij} \cos(\theta_i - \theta_j - \alpha_{ij}) = 0 \quad (14)$$

$$I_{di}V_i \cos(\delta_i - \theta_i) - I_{qi}V_i \sin(\delta_i - \theta_i) + Q_{Li} - \sum_{j \in S_B} V_i V_j Y_{ij} \sin(\theta_i - \theta_j - \alpha_{ij}) = 0, \quad (15)$$

where P_{Li} and Q_{Li} are, respectively, the active and reactive load, and $Y_{ij}e^{j\alpha_{ij}}$ is the entry of the admittance matrix.

For a non-generator bus $i \in S_L$, there are

$$P_{Li} - \sum_{j \in S_B} V_i V_j Y_{ij} \cos(\theta_i - \theta_j - \alpha_{ij}) = 0 \quad (16)$$

$$Q_{Li} - \sum_{j \in S_B} V_i V_j Y_{ij} \sin(\theta_i - \theta_j - \alpha_{ij}) = 0, \quad (17)$$

where S_L is the set of non-generator buses and $S_B = S_G \cup S_L$ is the set of all of the buses.

C. Linearization of Dynamic System Model

Linearization of (5)–(17) yields

$$\Delta \dot{\mathbf{s}} = \mathbf{A}_1 \Delta \mathbf{s} + \mathbf{B}_1 \Delta \mathbf{I}_g + \mathbf{B}_2 \Delta \mathbf{V}_g + \mathbf{E}_1 \Delta \mathbf{u} \quad (18)$$

$$0 = \mathbf{C}_1 \Delta \mathbf{s} + \mathbf{D}_1 \Delta \mathbf{I}_g + \mathbf{D}_2 \Delta \mathbf{V}_g \quad (19)$$

$$0 = \mathbf{C}_2 \Delta \mathbf{s} + \mathbf{D}_3 \Delta \mathbf{I}_g + \mathbf{D}_4 \Delta \mathbf{V}_g + \mathbf{D}_5 \Delta \mathbf{V}_1 \quad (20)$$

$$0 = \mathbf{D}_6 \Delta \mathbf{V}_g + \mathbf{D}_7 \Delta \mathbf{V}_1, \quad (21)$$

where (18) is obtained by linearizing the differential equations (5)–(8) and (11)–(13), (19) comes from the stator algebraic equations (9)–(10), (20) comes from the network equations (14)–(15), and (21) is from the network equations (16)–(17); \mathbf{A}_1 , \mathbf{B}_1 , \mathbf{B}_2 , \mathbf{E}_1 , \mathbf{C}_1 , \mathbf{D}_1 , \mathbf{D}_2 , \mathbf{C}_2 , \mathbf{D}_3 are block diagonal matrices, \mathbf{D}_4 , \mathbf{D}_5 , \mathbf{D}_6 , \mathbf{D}_7 are full matrices, and

$$\begin{aligned} \mathbf{s}_i &= [\delta_i \ \omega_i \ E'_{qi} \ E'_{di} \ E_{fdi} \ V_{Ri} \ R_{Fi}]^\top & i \in S_G \\ \mathbf{I}_{gi} &= [I_{di} \ I_{qi}]^\top & i \in S_G \\ \mathbf{V}_{gi} &= [\theta_i \ V_i]^\top & i \in S_G \\ \mathbf{V}_{li} &= [\theta_i \ V_i]^\top & i \in S_L \\ \mathbf{u}_i &= [T_{Mi} \ V_{refi}]^\top & i \in S_G. \end{aligned}$$

We can rewrite (18)–(21) in the compact form (3), and

$$\mathbf{y} = [\mathbf{I}_g^\top \ \mathbf{V}_g^\top \ \mathbf{V}_1^\top]^\top$$

$$\tilde{\mathbf{A}} = \mathbf{A}_1, \quad \tilde{\mathbf{B}} = [\mathbf{B}_1 \ \mathbf{B}_2 \ \mathbf{0}],$$

$$\tilde{\mathbf{C}} = \begin{bmatrix} \mathbf{C}_1 \\ \mathbf{C}_2 \\ \mathbf{0} \end{bmatrix}, \quad \tilde{\mathbf{D}} = \begin{bmatrix} \mathbf{D}_1 & \mathbf{D}_2 & \mathbf{0} \\ \mathbf{0} & \mathbf{D}_6 & \mathbf{D}_7 \end{bmatrix}.$$

III. SMALL-SIGNAL STABILITY CONSTRAINT AND EIGENVALUE SENSITIVITIES

If the eigenvalues of the state matrix \mathbf{A} all have negative real parts, the power system is stable in small-signal stability sense. An index η called *spectral abscissa*, which is the largest real part of the eigenvalues, is often used to describe the security margin:

$$\eta(\mathbf{A}) = \max\{\text{Re}(\lambda) : \lambda \in \boldsymbol{\lambda}(\mathbf{A})\} = \text{Re}(\lambda_\eta), \quad (22)$$

where $\boldsymbol{\lambda}(\mathbf{A})$ represents all the eigenvalues of \mathbf{A} , $\text{Re}(\lambda)$ is the real parts of the eigenvalues λ , and λ_η is the eigenvalue with the largest real part. The spectral abscissa determines the decay rate of the amplitude of the oscillation. The smaller the spectral abscissa, the more stable the system is.

The state matrix \mathbf{A} usually has complex eigenvalues due to its unsymmetrical characteristic. Generally, the spectral abscissa function is non-smooth [17]. Fortunately, the spectral abscissa function has been proved to be locally Lipschitz and continuously differentiable on open dense subsets of \mathbb{R}^n [18], which means that it is continuously differentiable almost everywhere and its gradient can be easily obtained where it is defined by calculating first-order spectral abscissa sensitivities.

As for computing the spectral abscissa sensitivities, the numerical differentiation method is widely used, which performs eigenvalue analysis to get the spectral abscissa $\eta(\mathbf{A})$ of the state matrix at the equilibrium point and then vary one variable x_i by a small quantity ε to get the perturbed state matrix \mathbf{A}_ε and its spectral abscissa $\eta(\mathbf{A}_\varepsilon)$. The spectral abscissa sensitivity with respect to x_i can be approximated by

$$\frac{\partial \eta}{\partial x_i} \approx \frac{\eta(\mathbf{A}_\varepsilon) - \eta(\mathbf{A})}{\varepsilon}. \quad (23)$$

The numerical differentiation method is easy to implement, but for large systems its calculation burden can be heavy due to the repetitive procedure. Also, the sensitivity with respect to the power of the slack bus cannot be obtained. Alternatively, the spectral abscissa sensitivity can be obtained by closed-form formulas. Specifically, the j th eigenvalue sensitivity with respect to the i th variable x_i can be written as [12], [13]:

$$\frac{\partial \lambda_j}{\partial x_i} = \frac{\boldsymbol{\psi}_j \frac{\partial \mathbf{A}}{\partial x_i} \boldsymbol{\phi}_j}{\boldsymbol{\psi}_j \boldsymbol{\phi}_j}, \quad (24)$$

where $\boldsymbol{\psi}_j$ and $\boldsymbol{\phi}_j$ are, respectively, the left and right eigenvectors of the eigenvalue λ_j , and

$$\begin{aligned} \frac{\partial \mathbf{A}}{\partial x_i} &= \frac{\partial \tilde{\mathbf{A}}}{\partial x_i} - \frac{\partial \tilde{\mathbf{B}}}{\partial x_i} \tilde{\mathbf{D}}^{-1} \tilde{\mathbf{C}} \\ &+ \tilde{\mathbf{B}} \tilde{\mathbf{D}}^{-1} \frac{\partial \tilde{\mathbf{D}}}{\partial x_i} \tilde{\mathbf{D}}^{-1} \tilde{\mathbf{C}} - \tilde{\mathbf{B}} \tilde{\mathbf{D}}^{-1} \frac{\partial \tilde{\mathbf{C}}}{\partial x_i}. \end{aligned} \quad (25)$$

Then the sensitivity of the spectral abscissa with respect to x_i can be given by

$$\frac{\partial \eta}{\partial x_i} = \text{Re} \left(\frac{\partial \lambda_\eta}{\partial x_i} \right). \quad (26)$$

From (25) it is seen that the derivation of the eigenvalue sensitivities for all of the variables requires considerable work since the elements of $\tilde{\mathbf{A}}$, $\tilde{\mathbf{B}}$, $\tilde{\mathbf{C}}$, and $\tilde{\mathbf{D}}$ can be different functions of several variables. However, the derivation is

required only once. In this paper, we use the closed-form formulation to compute the gradient of the spectral abscissa.

IV. A SEQUENTIAL QUADRATIC PROGRAMMING ALGORITHM COMBINED WITH GRADIENT SAMPLING

Sequential Quadratic Programming (SQP) has a long and rich history in solving smooth constrained optimization problems [19]. In each iterate of the traditional SQP algorithms, a quadratic programming (QP) subproblem is solved to obtain a search direction. However, the traditional SQP algorithms will fail for nonsmooth problems in theory and in practice. In 2005 an algorithm known as Gradient Sampling (GS) was developed for nonsmooth unconstrained optimization problems [20]. More recently, a SQP-GS method that combines the techniques of SQP and GS is developed [15], which is proved to be able to globally convergent to stationary points with probability one when the objective and constraint functions are locally Lipschitz and continuously differentiable on open dense subsets of \mathbb{R}^n . SQP-GS has been shown to be a reliable method for many challenging nonsmooth problems, even when the objective function is not locally Lipschitz, in which case the convergence cannot be guaranteed though [15].

The GS algorithm is conceptually simple. Basically, it is a stabilized steepest descent algorithm [21]. In each iteration, a descent direction is obtained by evaluating the gradient of the objective function at the current iterate and an additional set of nearby points and computing the vector in the convex hull of the gradients with the smallest norm. A standard line search is then used to obtain a lower point. The stabilization is controlled by the gradient sampling radius. As a natural extension to constrained optimization, the GS procedure samples the gradients of the constraint functions along with the objective function, thereby ensuring that good search directions are produced in nonsmooth regions.

Generally, the SQP-GS algorithm is developed to solve optimization problems in the following form:

$$\begin{aligned} \min_{\mathbf{x}} \quad & f(\mathbf{x}) \\ \text{s.t.} \quad & \mathbf{h}(\mathbf{x}) = 0 \\ & \underline{\mathbf{g}} \leq \mathbf{g}(\mathbf{x}) \leq \bar{\mathbf{g}}, \end{aligned} \quad (27)$$

where the objective function $f : \mathbb{R}^n \rightarrow \mathbb{R}$, the equality constraint functions $\mathbf{h} : \mathbb{R}^n \rightarrow \mathbb{R}^s$, and the inequality constraint functions $\mathbf{g} : \mathbb{R}^n \rightarrow \mathbb{R}^m$ are locally Lipschitz and continuously differentiable on open dense subsets of \mathbb{R}^n .

At the heart of SQP-GS is the following QP used to compute a search direction in the k th iteration:

$$\min_{\mathbf{d}, z, \mathbf{e}, \bar{\mathbf{r}}, \underline{\mathbf{r}}} \quad \rho z + \sum_{j=1}^{m_g} (\bar{\mathbf{r}}^j + \underline{\mathbf{r}}^j) + \sum_{i=1}^{m_h} e^i + \frac{1}{2} \mathbf{d}_k^\top \mathbf{H}_k \mathbf{d}_k \quad (28)$$

$$\text{s.t.} \quad f(\mathbf{x}_k) + \nabla f(\mathbf{x}_k)^\top \mathbf{d}_k \leq z \quad \forall \mathbf{x} \in \mathcal{B}_{\epsilon, k}^f \quad (29)$$

$$h^i(\mathbf{x}_k) + \nabla h^i(\mathbf{x}_k)^\top \mathbf{d}_k \leq e^i \quad \forall \mathbf{x} \in \mathcal{B}_{\epsilon, k}^{h^i} \quad (30)$$

$$-h^i(\mathbf{x}_k) - \nabla h^i(\mathbf{x}_k)^\top \mathbf{d}_k \leq -e^i \quad \forall \mathbf{x} \in \mathcal{B}_{\epsilon, k}^{h^i} \quad (31)$$

$$g^j(\mathbf{x}_k) + \nabla g^j(\mathbf{x}_k)^\top \mathbf{d}_k \leq \bar{\mathbf{r}}^j + \bar{\mathbf{g}}^j \quad \forall \mathbf{x} \in \mathcal{B}_{\epsilon, k}^{g^j} \quad (32)$$

$$-g^j(\mathbf{x}_k) - \nabla g^j(\mathbf{x}_k)^\top \mathbf{d}_k \leq \underline{\mathbf{r}}^j - \underline{\mathbf{g}}^j \quad \forall \mathbf{x} \in \mathcal{B}_{\epsilon, k}^{g^j} \quad (33)$$

$$(\mathbf{e}, \bar{\mathbf{r}}, \underline{\mathbf{r}}) \geq 0, \quad (34)$$

where ρ is a penalty parameter, \mathbf{d}_k is the search direction, \mathbf{H}_k is the approximated Hessian of the Lagrangian of (27), m_h and m_g are, respectively, the number of the equality and inequality constraints, z , \mathbf{e} , $\bar{\mathbf{r}}$, and $\underline{\mathbf{r}}$ are slack variables, and

$$\mathcal{B}_{\epsilon, k}^f := \{\mathbf{x}_{k,0}^f, \mathbf{x}_{k,1}^f, \dots, \mathbf{x}_{k,p}^f\}, \text{ where } \mathbf{x}_{k,0}^f := \mathbf{x}_k \quad (35)$$

$$\mathcal{B}_{\epsilon, k}^{h^i} := \{\mathbf{x}_{k,0}^{h^i}, \mathbf{x}_{k,1}^{h^i}, \dots, \mathbf{x}_{k,p}^{h^i}\}, \text{ where } \mathbf{x}_{k,0}^{h^i} := \mathbf{x}_k \quad (36)$$

$$\mathcal{B}_{\epsilon, k}^{g^j} := \{\mathbf{x}_{k,0}^{g^j}, \mathbf{x}_{k,1}^{g^j}, \dots, \mathbf{x}_{k,p}^{g^j}\}, \text{ where } \mathbf{x}_{k,0}^{g^j} := \mathbf{x}_k \quad (37)$$

are sets of p (sample size) independent and identically distributed random points uniformly sampled from

$$\mathbb{B}_\epsilon(\mathbf{x}_k) := \|\mathbf{x} - \mathbf{x}_k\|_2 \leq \epsilon, \quad (38)$$

where ϵ is the sample radius. To indicate the progress of the algorithm iterations, an infeasibility vector is defined as

$$\boldsymbol{\sigma}_k(\mathbf{x}_k) := \begin{pmatrix} |\mathbf{h}(\mathbf{x}_k)| \\ \max(\mathbf{g}(\mathbf{x}_k) - \bar{\mathbf{g}}, 0) \\ \max(\underline{\mathbf{g}} - \mathbf{g}(\mathbf{x}_k), 0) \end{pmatrix}. \quad (39)$$

The following model reduction is also defined in terms of primal and dual infeasibility, which can be zero only if \mathbf{x}_k is ϵ -stationary [15]:

$$\begin{aligned} \Delta \mathbf{q}_k := & \rho f(\mathbf{x}_k) + \sum \boldsymbol{\sigma}_k(\mathbf{x}_k) - \rho \max_{\mathbf{x} \in \mathcal{B}_{\epsilon, k}^f} \{f(\mathbf{x}_k) + \nabla f(\mathbf{x})^\top \mathbf{d}_k\} \\ & - \frac{1}{2} \mathbf{d}_k^\top \mathbf{H}_k \mathbf{d}_k - \sum_{i=1}^{m_h} \max_{\mathbf{x} \in \mathcal{B}_{\epsilon, k}^{h^i}} |h^i(\mathbf{x}_k) + \nabla h^i(\mathbf{x})^\top \mathbf{d}_k| \\ & - \sum_{j=1}^{m_g} \max_{\mathbf{x} \in \mathcal{B}_{\epsilon, k}^{g^j}} \{ \max\{g^j(\mathbf{x}_k) + \nabla g^j(\mathbf{x})^\top \mathbf{d}_k - \bar{\mathbf{g}}^j, 0\} \\ & - \max\{-g^j(\mathbf{x}_k) - \nabla g^j(\mathbf{x})^\top \mathbf{d}_k + \underline{\mathbf{g}}^j, 0\} \}. \end{aligned} \quad (40)$$

Then the SQP-GS algorithm is presented in Algorithm 1.

The SQP-GS algorithm generalizes the traditional SQP method to nonsmooth constrained problems. When solving a smooth constrained problem, the sample size p can be chosen as zero, in which case the SQP-GS algorithm reduces to the traditional SQP method.

If a function is known to be continuously differentiable everywhere in \mathbb{R}^n , it is unnecessary to sample its gradient at nearby points. This can significantly improve the performance of the algorithm because the evaluation of the linear inequality constraints from the quadratic programming can be largely eliminated. Besides, for those functions that depend on fewer than n variables, sampling fewer points can still yield good results. Also, since the points are sampled independently, it allows to use parallel computing to further reduce CPU time.

V. SOLVING SSSC-OPF BY SQP-GS

Here we discuss how to apply the SQP-GS algorithm in Section IV to solve the SSSC-OPF problem.

Algorithm 1 SQP-GS Algorithm

1: **Initialization:** Set $k = 1$, $K_{\max} = 100$; Choose a sampling radius $\epsilon > 0$, penalty parameter $\rho > 0$, constraint violation tolerance $\tau > 0$, sample size $p > 0$, line search constant $\varpi \in (0, 1)$, backtracking constant $\gamma \in (0, 1)$, sampling radius reduction factor $\mu_\epsilon \in (0, 1)$, penalty parameter reduction factor $\mu_\rho \in (0, 1)$, constraint violation tolerance reduction factor $\mu_\tau \in (0, 1)$, infeasibility tolerance $\nu_{in} > 0$, and stationarity tolerance parameter $\nu_s > 0$. Choose an initial iterate \mathbf{x} .

2: **while** $k < K_{\max}$

3: **if** $\max(\Delta \mathbf{q}_k) < \nu_s$ and $\max(\boldsymbol{\sigma}_k) < \nu_{in}$

4: Output solution and stop.

5: **end if**

6: **Gradient sampling:** Generate $\mathcal{B}_{\epsilon,k}^f$, $\mathcal{B}_{\epsilon,k}^h$, and $\mathcal{B}_{\epsilon,k}^g$ by (35)–(38).

7: **Search direction calculation:** Solve (28)–(34) to get $(\mathbf{d}_k, \mathbf{z}_k, \bar{\mathbf{r}}_k, \underline{\mathbf{r}}_k, \mathbf{e}_k)$.

8: **L-BFGS update:** Limited-memory Broyden-Fletcher-Goldfarb-Shanno (L-BFGS) method [22] that is typical in smooth optimization is used to update \mathbf{H}_k .

9: **if** $\Delta \mathbf{q}_k > \nu_s \epsilon^2$

10: **go** to step 20.

11: **else**

12: **if** $\max(\boldsymbol{\sigma}_k) \leq \tau$

13: **set** $\tau \leftarrow \mu_\tau \tau$

14: **else**

15: **set** $\rho \leftarrow \mu_\rho \rho$

16: **end if**

17: **set** $\epsilon \leftarrow \mu_\epsilon \epsilon$, $\beta_k \leftarrow 0$

18: **go** to step 21

19: **end if**

20: **Line search:** Set β_k as the largest value in the sequence $\{1, \gamma, \gamma^2, \dots\}$ such that $\mathbf{x}_{k+1} \leftarrow \mathbf{x}_k + \beta_k \mathbf{d}_k$ satisfies:

$$\rho f(\mathbf{x}_{k+1}) + \sum \boldsymbol{\sigma}_k(\mathbf{x}_{k+1}) \leq \rho f(\mathbf{x}_k) + \sum \boldsymbol{\sigma}_k(\mathbf{x}_k) - \varpi \beta_k \Delta \mathbf{q}_k \quad (41)$$

21: **Iteration increment:** Set $k \leftarrow k + 1$

22: **end do**

A. Model of SSSC-OPF

The model of SSSC-OPF is actually a ‘standard’ OPF model defined as a smooth nonlinear programming problem with an additional small-signal stability constraint. Specifically, the SSSC-OPF model can be represented as follows.

- 1) Minimizing the generation cost is usually considered as the objective function

$$f = \sum_{i \in S_G} (a_{2i} P_{Gi}^2 + a_{1i} P_{Gi} + a_{0i}), \quad (42)$$

where P_{Gi} is the active power output of the i th generator, and a_{2i} , a_{1i} , and a_{0i} are the corresponding cost coefficients.

- 2) Power flow equations for bus $i \in S_B$

$$P_{Gi} - P_{Li} - \sum_{j \in i} V_i Y_{ij} V_j \cos(\theta_i - \theta_j - \alpha_{ij}) = 0 \quad (43)$$

$$Q_{Gi} - Q_{Li} - \sum_{j \in i} V_i Y_{ij} V_j \sin(\theta_i - \theta_j - \alpha_{ij}) = 0, \quad (44)$$

where Q_{Gi} is the reactive power output of the i th generator.

- 3) Initial condition equations for generator $i \in S_G$ with a two-axis model.

- Stator algebraic equations

$$E'_{di} - V_i \sin(\delta_i - \theta_i) - R_{si} I_{di} + X'_{qi} I_{qi} = 0 \quad (45)$$

$$E'_{qi} - V_i \cos(\delta_i - \theta_i) - R_{si} I_{qi} - X'_{di} I_{di} = 0. \quad (46)$$

- The generator terminal power can be obtained by the product of voltage and current transformed from d – q rotor reference frame to network reference frame as

$$P_{Gi} - V_i I_{di} \sin(\delta_i - \theta_i) - V_i I_{qi} \cos(\delta_i - \theta_i) = 0 \quad (47)$$

$$Q_{Gi} - V_i I_{di} \cos(\delta_i - \theta_i) + V_i I_{qi} \sin(\delta_i - \theta_i) = 0. \quad (48)$$

- In steady state, dE'_{qi}/dt in (7) and dE'_{di}/dt in (8) are zero and thus

$$E_{idi} - E'_{qi} - (X_{di} - X'_{di}) I_{di} = 0 \quad (49)$$

$$E'_{di} - (X_{qi} - X'_{qi}) I_{qi} = 0. \quad (50)$$

- 4) Technical constraints include

$$\underline{V}_i \leq V_i \leq \bar{V}_i \quad i \in S_B \quad (51)$$

$$\underline{P}_{Gi} \leq P_{Gi} \leq \bar{P}_{Gi} \quad i \in S_G \quad (52)$$

$$\underline{Q}_{Gi} \leq Q_{Gi} \leq \bar{Q}_{Gi} \quad i \in S_G \quad (53)$$

$$I_{ij}^2 \leq \bar{I}_{ij}^2 \quad (i, j) \in S_{\text{Line}}, \quad (54)$$

where I_{ij} is the current of line (i, j) , S_{Line} is the set of all lines and $\bar{(\cdot)}$ and $\underline{(\cdot)}$ denote the upper and lower limits.

- 5) Small-signal stability constraint:

$$\eta(\mathbf{x}) \leq \bar{\eta} \quad (55)$$

where $\mathbf{x} = [P_G^\top Q_G^\top V^\top \boldsymbol{\theta}^\top \boldsymbol{\delta}^\top E_d'^\top E_q'^\top I_d^\top I_q^\top E_{fd}^\top]^\top$ is the vector of variables in the model. The choice of $\bar{\eta}$ depends on the system characteristics and can be determined based on offline stability studies.

B. Employing SQP-GS to Solve SSSC-OPF

Obviously, the SSSC-OPF model belongs to the type of optimization problem in (27). Before employing the SQP-GS method that relies on the gradients to construct the QP subproblem, the gradients of all functions in the model with respect to \mathbf{x} , the variables of the model, should be derived. The objective function and constraint functions in (43)–(54) are smoothly nonlinear or linear, and their gradients with respect to \mathbf{x} can be easily derived. As discussed in Section III, the spectral abscissa function in (55) is implicit but the function value and its gradient can also be evaluated.

As discussed in Section IV, it is unnecessary to sample the gradients of the smooth functions. In SSSC-OPF, the function in (55) is the only nonsmooth function, and thus only its gradient need to be sampled, which requires the following steps for the k iteration:

- 1) **Sampling Points:** Generate p points $\mathcal{B}_{\epsilon,k}^\eta$ by (38).
- 2) **Eigenvalue Analysis:** Set up state matrix \mathbf{A} for each point $\mathbf{x} \in \mathcal{B}_{\epsilon,k}^\eta$ and calculate the most critical eigenvalue λ_η and the corresponding left and right eigenvectors ψ_η and ϕ_η for each \mathbf{A} ;
- 3) **Sensitivities:** Calculate the gradients $\partial\tilde{\mathbf{A}}/\partial x_i$, $\partial\tilde{\mathbf{B}}/\partial x_i$, $\partial\tilde{\mathbf{C}}/\partial x_i$, and $\partial\tilde{\mathbf{D}}/\partial x_i$ for each point with respect to the i th variable $x_i \in \mathbf{x}$; obtain the gradients $\partial\mathbf{A}/\partial x_i$ for each \mathbf{A} in terms of (25); and calculate the eigenvalue sensitivity $\partial\lambda_\eta/\partial x_i$ in (24) for $\mathbf{x} \in \mathcal{B}_{\epsilon,k}^\eta$.
- 4) **Gradient:** Get the gradient $\partial\eta/\partial x_i$ with respect to the i th variable $x_i \in \mathbf{x}$ referred to (26) for each point.

Note that the steps (2)–(4) can be performed in parallel.

VI. CASE STUDIES

The proposed method is applied to the WSCC 3-machine 9-bus, New England 10-machine 39-bus, and the modified IEEE 57-machine 118-bus systems to illustrate the effectiveness in solving SSSC-OPF. For all systems, the generators are described by the two-axis model with an IEEE type-I exciter. The loads are modeled as constant power.

The SQP-GS method is implemented in MATLAB by using CPLEX 12.60 [23] as the QP solver for the subproblem. The eigenvalues and eigenvectors are computed by QR decomposition using the MATLAB function *eig*. Flat start is used for which all voltage angles are set to be zero, all voltage magnitudes are set to be 1.0 p.u., $P_G = (\overline{P}_G + \underline{P}_G)/2$, and $Q_G = (\overline{Q}_G + \underline{Q}_G)/2$. The parameters of SQP-GS are chosen as $\rho = 0.1$, $\mu_\rho = 0.5$, $\epsilon = 0.1$, $\mu_\epsilon = 0.5$, $\tau = 0.1$, $\mu_\tau = 0.8$, $\varpi = 1$, $\gamma = 0.8$ from [15]. The tolerances ν_{in} and ν_s are set to be 10^{-3} and 10^{-2} , respectively.

A. WSCC 3-Machine 9-Bus System

The WSCC 9-bus system is often used for stability analysis [6]. The system data, including power limit and security data can be found [14]. The generator cost coefficients are listed in Table I. To analyze the effectiveness of the proposed method, we consider the following three cases:

- 1) *Case 0:* Base case, which is a standard OPF without any small-signal stability constraint.
 - 2) *Case 1:* SSSC-OPF without any binding small-signal stability constraint.
 - 3) *Case 2:* SSSC-OPF with a binding small-signal stability constraint.
- **Case 0:** We use IPM to solve the standard OPF without small-signal stability constraint and the results are listed in the first row of Table II. The eigenvalue analysis is performed and the spectral abscissa η is -0.04 .
 - **Case 1:** A security margin $\bar{\eta} = -0.01$ is used, which is larger than the spectral abscissa in the base case. Since the small-signal stability constraint is not binding in this

TABLE I
GENERATION COST COEFFICIENTS FOR WSCC 9-BUS SYSTEM

Generator#	$a_2, \$/(\text{MW})^2$	$a_1, \$/\text{MW}$	$a_0, \$$
1	9.76×10^{-4}	14.712	0.00
2	7.20×10^{-4}	11.290	0.00
3	5.46×10^{-4}	8.001	0.00

case, the problem can be successfully solved by the SQP method without gradient sampling and the results are the same as those in the base case.

- **Case 2:** $\bar{\eta}$ is set to be three different values, all of which are less than the spectral abscissa in the base case. When $\bar{\eta}$ is set to be -0.45 or -0.5 , the SQP will not converge without a GS procedure. Here the sample size is chosen as 10. From Table II it is seen that the power outputs of the generators are re-dispatched to satisfy the small-signal stability constraint. Also, the more binding the small-signal stability constraint, the more expensive the generation cost is. As $\bar{\eta}$ decreases, the active power generated by generator G3 which has the cheapest generation cost gradually goes down, mainly because G3 has the smallest inertial constant and generating more power from the other two generators can help improve the stability. When $\bar{\eta} = -0.5$, the re-dispatch from SSSC-OPF will allow significantly more generation from G1 which has the most expensive generation cost but the largest inertial constant.

B. New England 10-Machine 39-Bus System

The full dynamic data of the New England 10-machine 39-bus system are extracted from [24] and the economic and technical data are from [9]. For the voltage magnitude limits, we choose $\overline{V} = 1.1$ p.u. and $\underline{V} = 0.9$ p.u. for all buses. For standard OPF, the spectral abscissa $\eta = -0.11$. To reduce the spectral abscissa, the SSSC-OPF is applied with $\bar{\eta} = -0.2$.

The SSSC-OPF is calculated by SQP-GS with no samples, 30 samples, and 60 samples, respectively. As in Fig. 1, the infeasibility defined in (39) cannot reduce to the tolerance with 100 iterations when the sample size is 0. By contrast, when the sample size is 30 or 60, the infeasibility reduces to $\nu_{in} = 10^{-3}$ rapidly. Also, as shown in Fig. 2, the model reduction defined in (40) decreases to an acceptable tolerance with sampling gradients. In Fig. 3 we show the generation cost which stably approaches an optimal value. From Figs. 1–3, we can see that the gradient sampling plays an important role in solving the SSSC-OPF problems. Moreover, based on our tests, the GS with 30 samples are good enough to improve the search direction of SQP for the SSSC-OPF problem.

We also compare SQP-GS with the numerical eigenvalue sensitivity based IPM (IPM-NES) [9] and the results are listed in Table III, where \overline{P}_G is the maximum active power output of a generator. The results for the OPF without small signal stability constraint (denoted by ‘OPF’) is also listed for reference. IPM-NES can also solve the problem but needs higher cost than SQP-GS to ensure the same level of small-signal stability. Comparing the generations of IPM-NES and SQP-GS, we can see that the generations of G3 and G5 are

TABLE II
SUMMARY OF SSSC-OPF RESULTS WITH DIFFERENT SMALL-SIGNAL CONSTRAINTS FOR WSCC 3-MACHINE 9-BUS SYSTEM

	Generation Cost (\$/h)	η	P_{G1} (MW)	P_{G2} (MW)	P_{G3} (MW)	V_1 (pu)	V_2 (pu)	V_3 (pu)
Base Case	2901.3	-0.04	25.0	25.0	276.0	1.040	1.045	1.022
Case 1 ($\eta \leq -0.01$)	2901.3	-0.04	25.0	25.0	276.0	1.040	1.045	1.022
Case 2 ($\eta \leq -0.30$)	2919.7	-0.30	25.0	47.1	252.4	1.040	1.045	1.045
Case 2 ($\eta \leq -0.45$)	2957.5	-0.45	25.0	59.8	239.3	1.026	1.045	1.045
Case 2 ($\eta \leq -0.50$)	3217.9	-0.50	84.4	25.0	211.8	0.997	1.045	1.022

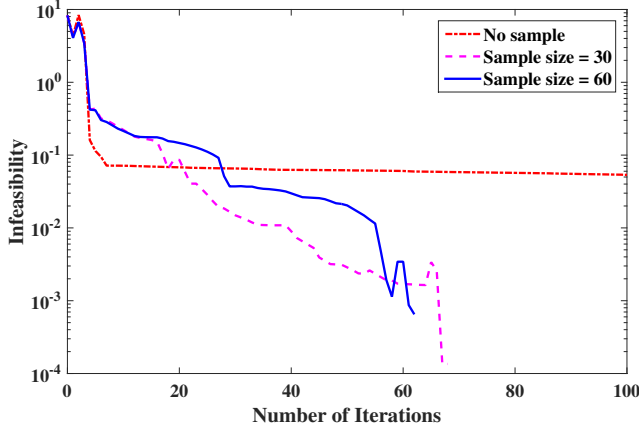


Fig. 1. Infeasibility curve for IEEE 39-bus system.

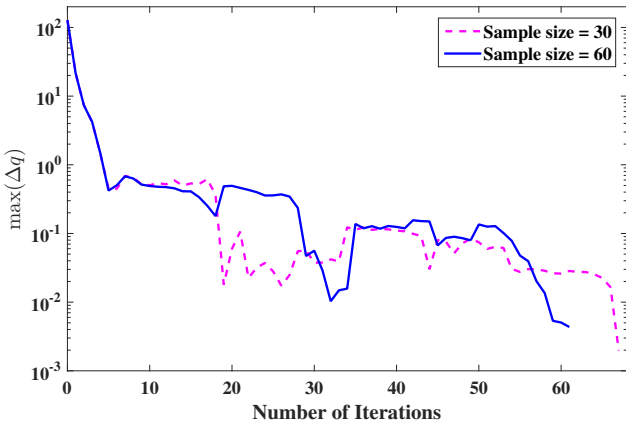


Fig. 2. Model reduction curve for IEEE 39-bus system.

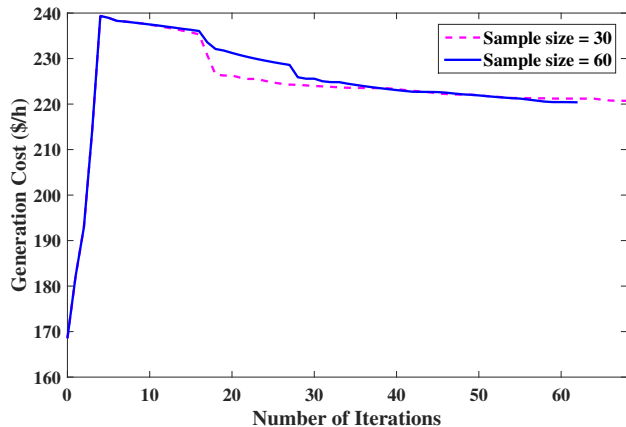


Fig. 3. Objective curve for IEEE 39-bus system.

the same while there are significant differences for the other generators. Actually the active power outputs of G3 and G5 always reach the maximum power output in all methods, which is mainly due to their much cheaper generation cost.

The critical modes that change in the first 10 iterations for both methods are listed in Table IV. We can see that after 5 iterations SQP-GS moves to the binding critical modes for small-signal stability constraint and stays in this mode until convergence. However, IPM-NES gets the same mode at the 3rd and 10th iteration but suffers from oscillations between some critical modes during iterations.

TABLE III
COMPARISON BETWEEN SQP-GS AND IPM-NES FOR 39-BUS SYSTEM

	SQP-GS (MW)	IPM-NES (MW)	OPF (MW)	\bar{P}_G (MW)
G1	0.00	402.5	0.00	402.5
G2	698.8	132.4	747.5	747.5
G3	920.0	920.0	920.0	920.0
G4	298.8	100.8	0.00	862.5
G5	747.5	747.5	747.5	747.5
G6	740.0	479.8	862.5	862.5
G7	342.3	862.5	0.00	862.5
G8	557.1	181.8	805.0	805.0
G9	804.3	1000.4	883.3	1035.0
G10	1047.1	1308.8	1195.0	1380.0
Cost (\$/h)	220.7	239.1	213.9	-

C. IEEE 54-Machine 118-Bus System

We also test the proposed method on a modified version of the IEEE 54-machine 118-bus benchmark system with dynamic data from [25]. This system has 54 synchronous machines with IEEE type-1 exciters, 20 of which are synchronous compensators used only for reactive power support and 15 of which are motors. For a standard OPF, the spectral abscissa $\eta = 0.35$. We set $\bar{\eta}$ to be -0.1 . The voltage magnitudes at all buses must be between 0.9 p.u. and 1.1 p.u. . The reactive power limits can be found in [26].

IPM-NES fails to solve this problem. By contrast, SQP-GS only needs 13 and 12 iterations to solve the problem, respectively, when there are 30 samples and 60 samples. The generation cost of SSSC-OPF will increase to 6110.8\$/h from 5779.2\$/h for the standard OPF with $\eta = 0.35$.

Since eigenvalue analysis and the SSSC-OPF use the linearized system model, they cannot take into account the full nonlinear behavior of the power system. Therefore, in order to

further validate the solution of SSSC-OPF from SQP-GS, we increase the load at bus 2 by 5 MW and perform time-domain simulation using the full nonlinear power system model for the operating states obtained from both the standard OPF and SSSC-OPF. The rotor frequencies of all generators for the standard OPF and SSSC-OPF are shown in Figs. 4 and 5, respectively. It is seen that under the standard OPF the system is unstable while under SSSC-OPF the oscillation can be quickly damped.

TABLE IV
CRITICAL MODES IN 10 ITERATIONS FOR 39-BUS SYSTEM

Iter.	SQP-GS	IPM-NES
1	-0.1193 ± j0.4060	-0.0965 ± j 0.5086
	-0.1389 ± j0.3919	-0.1537 ± j0.5302
	-0.1664 ± j0.4264	-0.1869 ± j0.7166
	-0.1773 ± j4.1030	-0.1876 ± j6.2010
2	-0.1394 ± j0.4056	-0.1860 ± j0.7117
	-0.1597 ± j0.4263	-0.1935 ± j3.9960
	-0.1706 ± j0.4484	-0.1965 ± j7.5179
	-0.1836 ± j4.3023	-0.2010 ± j6.0230
3	-0.1578 ± j0.4271	-0.1776 ± j6.1767
	-0.1799 ± j0.4217	-0.1888 ± j3.9706
	-0.1865 ± j4.4437	-0.2102 ± j7.5391
	-0.1994 ± j0.4592	-0.2104 ± j5.4174
4	-0.1762 ± j0.4374	-0.1768 ± j4.0281
	-0.1837 ± j4.5249	-0.1917 ± j6.1061
	-0.1842 ± j0.4306	-0.2035 ± j7.5423
	-0.1987 ± j6.9051	-0.2069 ± j0.6721
5	-0.1872 ± j6.8941	-0.1815 ± j4.0092
	-0.1895 ± j0.4458	-0.1945 ± j6.1100
	-0.1904 ± j4.4475	-0.2036 ± j7.5421
	-0.1970 ± j0.4421	-0.2066 ± j0.6721
6	-0.1829 ± j6.6878	-0.1865 ± j3.9870
	-0.1921 ± j4.2950	-0.1918 ± j6.1391
	-0.1948 ± j0.4488	-0.2031 ± j7.5365
	-0.2021 ± j0.4487	-0.2069 ± j0.6708
7	-0.1835 ± j6.5399	-0.1873 ± j6.1417
	-0.1932 ± j4.2018	-0.1922 ± j3.9662
	-0.1938 ± j0.4522	-0.2032 ± j7.5364
	-0.2053 ± j0.4516	-0.2066 ± j0.6708
8	-0.1835 ± j6.5089	-0.1803 ± j4.0352
	-0.1938 ± j4.1797	-0.1887 ± j0.7124
	-0.1941 ± j0.4527	-0.1974 ± j7.5183
	-0.2060 ± j0.4525	-0.2015 ± j6.0104
9	-0.1838 ± j6.4765	-0.1871 ± j0.7118
	-0.1943 ± j0.4533	-0.1978 ± j7.5172
	-0.1946 ± j4.1570	-0.2035 ± j6.0243
	-0.2067 ± j0.4534	-0.2118 ± j5.4177
10	-0.1841 ± j6.4444	-0.1776 ± j6.1778
	-0.1955 ± j4.1341	-0.2059 ± j5.4403
	-0.2075 ± j0.4542	-0.2095 ± j7.5394
	-0.2080 ± j0.6288	-0.2164 ± j3.8262

Since the sampling in SQP-GS is random, the solutions may be different for different runs. We run SQP-GS for 20 times and the standard deviation of the generation cost is 0.06 \$/h. In Fig. 6 we show the coefficient of variation, the standard deviation divided by the mean, of the generation output for each generator over 20 runs, which is very small and indicates that the difference between the solutions is small.

D. Efficiency

We also test the efficiency of the proposed method on 39- and 118-bus systems. All simulations are carried out on a Dell Precision T5810 with a four-core 3.5 GHz processor

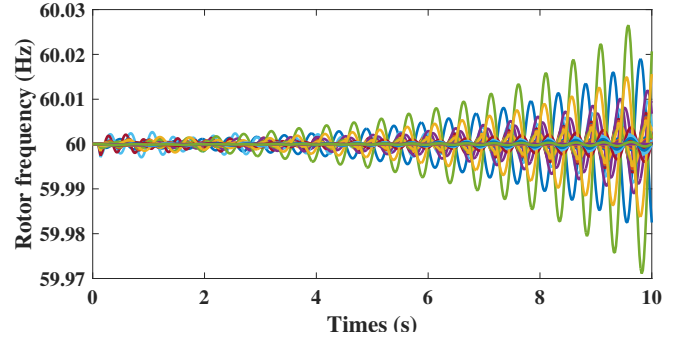


Fig. 4. Time-domain simulation of 118-bus system for standard OPF.

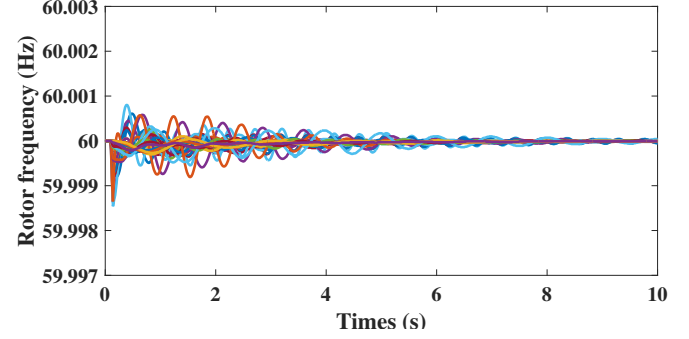


Fig. 5. Time-domain simulation of 118-bus system for SSSC-OPF.

and 64 GB RAM memory. Each iteration of the proposed method involves eigenvalue analysis, computing sensitivities, and solving QP subproblem.

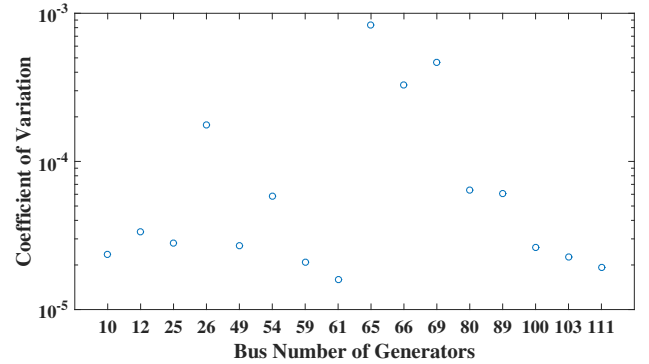


Fig. 6. Coefficient of variation of generation outputs for 118-bus system over 20 runs of SSSC-OPF.

Table V lists the average step and the total CPU time with sample size 30 and 60. It is seen that the proposed SQP-GS method can solve the SSSC-OPF problem efficiently. Since in each iteration the gradient sampling performs eigenvalue analysis and sensitivity calculation for many times, these two steps are time consuming. However, because the gradients can be sampled independently, the required CPU time can be greatly reduced by parallel computing. Furthermore, the computational burden of the eigenvalue analysis can be reduced by only calculating critical eigenvalues, such as by Jacobi-Davidson Method [27].

From Table V it is also seen that the number of iterations

TABLE V
CALCULATION TIME OF SQP-GS ON 39-BUS AND 118-BUS SYSTEMS

Step	New England 39-bus system						IEEE 118-bus system					
	Sample size = 30			Sample size = 60			Sample size = 30			Sample size = 60		
	CPU(s) /call	Calls /iter.	CPU(s) /iter.	CPU(s) /call	Calls /iter.	CPU(s) /iter.	CPU(s) /call	Calls /iter.	CPU(s) /iter.	CPU(s) /call	Calls /iter.	CPU(s) /iter.
Eigen. Analysis	0.004	32	0.13	0.004	62	0.24	0.103	32	3.29	0.108	65	7.05
Sensitivities	0.005	31	0.14	0.005	61	0.27	0.028	31	0.86	0.029	61	1.79
QP	0.12	1	0.12	0.14	1	0.14	0.62	1	0.62	0.72	1	0.72
Iter. Times	68			62			13			12		
Total CPU (s)	26.72 (8.97*)			40.60 (9.54*)			60.33 (9.94*)			114.93 (10.49*)		

*Estimated CPU time if ideal parallel techniques are used to sample the gradients

Estimated CPU time = (Eigen. Analysis CPU(s)/call + Sensitivities CPU(s)/call + QP CPU(s)/call) × Iter. Times + the other time.

The other time includes L-BFGS time in Step 8 of Algorithm 1, linear search time in Step 20 of Algorithm 1, and data input and result output time.

for the IEEE 118-bus system is smaller than that for the New England 39-bus system. The iteration times of SQP-GS can depend on the system size, the constraints, and the objective function. In our test cases it seems that the small-signal stability constraint is the dominant factor, and the IEEE 118-bus case has a smaller number of iterations mainly because its $\bar{\eta}$ in the small-signal stability constraint is greater than that in the New England 39-bus case ($\bar{\eta} = -0.1$ for IEEE 118-bus case and $\bar{\eta} = -0.2$ for New England 39-bus case).

VII. CONCLUSION

In this paper, we propose an SQP-GS method to solve the SSSC-OPF problem, which is a nonsmooth optimization problem due to the property of the spectral abscissa function. In SQP-GS, a GS technique is used to evaluate the gradients around the current iterate to make the search direction computation effective in the nonsmooth regions. The closed-form eigenvalue sensitivity is used to calculate the gradient of the spectral abscissa. Simulation results on three test systems show that the proposed method can solve the SSSC-OPF problem effectively without any convergence problem. By contrast, the existing Interior Point Method either cannot get as good solution as SQP-GS or even fail for relatively large systems.

REFERENCES

- [1] G. Rogers, *Power System Oscillation*. New York: Springer, 2000.
- [2] J. Quintero, V. Vittal, G. Heydt, and H. Zhang, "The impact of increased penetration of converter control-based generators on power system modes of oscillation," *IEEE Trans. Power Syst.*, vol. 29, no. 5, pp. 2248–2256, Sept. 2014.
- [3] T. Weckesser, H. Johannsson, and J. Ostergaard, "Real-time remedial action against aperiodic small signal rotor angle instability," *IEEE Trans. Power Syst.*, vol. 31, no. 1, pp. 387–396, Jan. 2016.
- [4] C. Wang, Y. Lv, H. Huang, J. Zhang, J. Li, Y. Li, W. Sun, and Y. Chang, "Low frequency oscillation characteristics of east china power grid after commissioning of huai-hu ultra-high voltage alternating current project," *J. Mod. Power Syst. Clean Energy*, vol. 3, no. 3, pp. 332–340, 2015.
- [5] C. Chung, L. Wang, F. Howell, and P. Kundur, "Generation rescheduling methods to improve power transfer capability constrained by small-signal stability," *IEEE Trans. Power Syst.*, vol. 19, no. 1, pp. 524–530, Feb. 2004.
- [6] P. W. Sauer and M. Pai, *Power system dynamics and stability*, 1st ed. Urbana-Champaign: Prentice Hall, 1998.
- [7] P. Kundur, N. J. Balu, and M. G. Lauby, *Power system stability and control*. New York: McGraw-hill, 1994.
- [8] Z. Yu, F. Li, L. Sun, X. Zhou, P. Zeng, and B. Li, "An on-line generation dispatching algorithm to improve small signal stability," in *2014 IEEE PES General Meeting — Conference Exposition*, Jul. 2014, pp. 1–5.
- [9] R. Zarate-Minano, F. Milano, and A. Conejo, "An OPF methodology to ensure small-signal stability," *IEEE Trans. Power Syst.*, vol. 26, no. 3, pp. 1050–1061, Aug. 2011.
- [10] S. Kodsí and C. Caizares, "Application of a stability-constrained optimal power flow to tuning of oscillation controls in competitive electricity markets," *IEEE Trans. Power Syst.*, vol. 22, no. 4, pp. 1944–1954, Nov. 2007.
- [11] J. Condren and T. Gedra, "Expected-security-cost optimal power flow with small-signal stability constraints," *IEEE Trans. Power Syst.*, vol. 21, no. 4, pp. 1736–1743, Nov. 2006.
- [12] F. Alvarado, C. DeMarco, I. Dobson, P. Sauer, S. Greene, H. Engdahl, and J. Zhang, "Avoiding and suppressing oscillations," *PSERC Project Final Report*, 1999.
- [13] H.-K. Nam, Y.-K. Kim, K.-S. Shim, and K. Lee, "A new eigen-sensitivity theory of augmented matrix and its applications to power system stability analysis," *IEEE Trans. Power Syst.*, vol. 15, no. 1, pp. 363–369, Feb. 2000.
- [14] P. Li, H. Wei, B. Li, and Y. Yang, "Eigenvalue-optimisation-based optimal power flow with small-signal stability constraints," *IET Gener. Transm. Dis.*, vol. 7, no. 5, pp. 440–450, May 2013.
- [15] F. E. Curtis and M. L. Overton, "A sequential quadratic programming algorithm for nonconvex, nonsmooth constrained optimization," *SIAM Journal on Optimization*, vol. 22, no. 2, pp. 474–500, 2012.
- [16] S. M. Deckmann and V. F. da Costa, "A power sensitivity model for electromechanical oscillation studies," *IEEE Transactions on Power Systems*, vol. 9, no. 2, pp. 965–971, May 1994.
- [17] A. S. Lewis and M. L. Overton, "Eigenvalue optimization," *Acta numerica*, vol. 5, pp. 149–190, 1996.
- [18] J. V. Burke and M. L. Overton, "Variational analysis of non-lipschitz spectral functions," *Mathematical Programming*, vol. 90, no. 2, pp. 317–351, 2001.
- [19] P. T. Boggs and J. W. Tolle, "Sequential quadratic programming," *Acta numerica*, vol. 4, pp. 1–51, 1995.
- [20] J. V. Burke, A. S. Lewis, and M. L. Overton, "A robust gradient sampling algorithm for nonsmooth, nonconvex optimization," *SIAM Journal on Optimization*, vol. 15, no. 3, pp. 751–779, 2005.
- [21] J. Nocedal and S. J. Wright, *Numerical Optimization*, 2nd ed. New York: Springer, 2006.
- [22] J. Nocedal, "Updating quasi-newton matrices with limited storage," *Mathematics of computation*, vol. 35, no. 151, pp. 773–782, 1980.
- [23] *CPLEX 12*, IBM ILOG CPLEX., 2013. [Online]. Available: <http://www-01.ibm.com/software/commerce/optimization/cplex-optimizer/>
- [24] R. H. Yeu, "Small signal analysis of power systems: Eigenvalue tracking method and eigenvalue estimation contingency screening for DSA," Ph.D. dissertation, University of Illinois at Urbana-Champaign, 2010.
- [25] "IEEE 118-bus modified test system," KIOS Research Center for Intelligent Systems and Networks of the University of Cyprus. [Online]. Available: <http://www.kios.ucy.ac.cy/testsystems/index.php/dynamic-ieee-test-systems/ieee-118-bus-modified-test-system>
- [26] "Power systems test case archive," Department of Electrical Engineering of the University of Washington. [Online]. Available: <https://www.ee.washington.edu/research/pstca/>
- [27] Z. Du, W. Liu, and W. Fang, "Calculation of rightmost eigenvalues in power systems using the jacobi-davidson method," *IEEE Trans. Power Syst.*, vol. 21, no. 1, pp. 234–239, Feb. 2006.



Peijie Li (M'14) received the B.E. degree and Ph.D. degree in electrical engineering from Guangxi University, Nanning, China, in 2006 and 2012, respectively.

From 2015, he is working at Argonne National Laboratory, Lemont, IL, USA, as a visiting scholar. He is currently also an associate professor at the Guangxi University. His research interests include optimal power flow, small-signal stability, security constrained economic dispatch and restoration.



Xiaoqing Bai received B.S. and Ph.D. degrees in power engineering from Guangxi University, Nanning, China, in 1991, 2010 respectively.

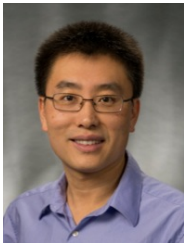
She was a Post Doctoral Research Assistant of University of Nebraska-Lincoln from 2012 to 2015. Now she is a Professor of Institute of Power System Optimization, Guangxi University. Her research interest is in power system optimization based on SDP and robust optimization.



Junjian Qi (S'12–M'13) received the B.E. degree from Shandong University, Jinan, China, in 2008 and the Ph.D. degree Tsinghua University, Beijing, China, in 2013, both in electrical engineering.

In February–August 2012 he was a Visiting Scholar at Iowa State University, Ames, IA, USA. During September 2013–January 2015 he was a Research Associate at Department of Electrical Engineering and Computer Science, University of Tennessee, Knoxville, TN, USA. Currently he is a Post-doctoral Appointee at the Energy Systems Division,

Argonne National Laboratory, Argonne, IL, USA. His research interests include cascading blackouts, power system dynamics, state estimation, synchrophasors, and cybersecurity.

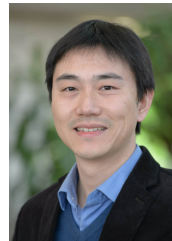


Jianhui Wang (M'07–SM'12) received the Ph.D. degree in electrical engineering from Illinois Institute of Technology, Chicago, IL, USA, in 2007.

Presently, he is the Section Lead for Advanced Power Grid Modeling at the Energy Systems Division at Argonne National Laboratory, Argonne, IL, USA.

Dr. Wang is the secretary of the IEEE Power & Energy Society (PES) Power System Operations Committee. He is an associate editor of Journal of Energy Engineering and an editorial board member

of Applied Energy. He is also an affiliate professor at Auburn University and an adjunct professor at University of Notre Dame. He has held visiting positions in Europe, Australia and Hong Kong including a VELUX Visiting Professorship at the Technical University of Denmark (DTU). Dr. Wang is the Editor-in-Chief of the IEEE Transactions on Smart Grid and an IEEE PES Distinguished Lecturer. He is also the recipient of the IEEE PES Power System Operation Committee Prize Paper Award in 2015.



Feng Qiu (M'14) received his Ph.D. from the School of Industrial and Systems Engineering at the Georgia Institute of Technology in 2013. He is a computational scientist with the Energy Systems Division at Argonne National Laboratory, Argonne, IL, USA. His current research interests include optimization in power system operations, electricity markets, and power grid resilience.



Hua Wei received BS and MS degrees in power engineering from Guangxi university, Guangxi, P.R. China in 1981 and 1987, respectively, and Ph.D. degree in power engineering from Hiroshima University, Japan in 2002.

He was a visiting Professor at Hiroshima University, Japan from 1994 to 1997. From 2004 to 2014, he was the vice-president of the Guangxi University. Now, he is a professor of Guangxi University. He is also the director of the Institute of Power System Optimization, Guangxi University. His research

interests include power system operation and planning, particularly in the application of optimization theory and methods to power systems.